Dalton Transactions

A Novel, Mesoporous Molybdenum Doped Titanium Dioxide/ Reduced Graphene Oxide Composite as a Green, Highly Efficient Solid Acid Catalyst for Acetalization

Journal:	*Dalton Transactions*
Manuscript ID	DT-ART-09-2019-003633.R4
Article Type:	Paper
Date Submitted by the Author:	27-Nov-2019
Complete List of Authors:	Thalgaspitiya, Wimalika; University of Connecticut, Department of Chemistry Kankanmkapuge, Tharindu; University of Connecticut, Department of Chemistry He, Junkai; University of Connecticut, Institute of Materials Science Kerns, Peter; University of Connecticut, Department of Chemistry Meguerdichian, Andrew; University of Connecticut, Institute of Materials Science Suib, Steven; University of Connecticut, Department of Chemistry; University of Connecticut, Institute of Materials Science

ARTICLE

A Novel, Mesoporous Molybdenum Doped Titanium Dioxide/ Reduced Graphene Oxide Composite as a Green, Highly Efficient Solid Acid Catalyst for Acetalization

Received 00th January 20xx,
Accepted 00th January 20xx

DOI: 10.1039/x0xx00000x

Wimalika R. K. Thalgaspitiya,[a] Tharindu Kankanam Kapuge,[a] Junkai He,[b] Peter Kerns,[a] Andrew Meguerdichian,[b] and Steven L. Suib*[a,b]

A novel , mesoporous composite of Mo doped TiO_2 / reduced graphene oxide is synthesized to be used as a highly efficient heterogeneous acid catalyst. The composite has a high surface area (263 m^2/g) and a monomodal pore size distribution with an average pore diameter of 3.4 nm. A comphrehensive characterization of the synthesized material was done using PXRD, Raman, BET, SEM, EDX, TEM, TGA, and XPS. The composite exhibited excellent catalytic activity (1.6 h^{-1} TOF, >99% GC yield, and >99% selectivity) towards acetalization of cyclohexanone at room tempertaure within 30 minutes. The catalyst was reusable up to 4 reaction cycles without any significant loss in the activity and the acidic site calculations showed that the reaction is mostly driven by the weak acidic sites on the composite.

Introduction

The use of solid acid catalysts has become popular as the conventional acid catalytic processes involve issues such as corrosiveness, safety hazards, production of harmful by products, and product separation difficulties.[1] The first application of a solid acid catalyst was introduced by Houdry[2] in the late 1930's and later several different classes of solid acids namely zeolites,[3–5] oxides,[6,7] mixed oxides,[8,9] heteropoly acids,[10,11] molecular sieves,[12] phosphates,[13,14] and organic-inorganic hybrids[15] were reported. However, the use of most solid acid catalysts is limited to reactions where water is present due to their inactivation by strong chemisorption of water on the surface and solubility.[16] Thus the need of water resistant solid catalysts has become important to make industrial processes environmentally benign as most of the industries still use conventional acids such as H_2SO_4.

As highly efficient water resistant solid acid catalysts, functionalized carbonaceous materials were introduced due to their tuneable properties and stability in different media (acidic/basic).[1] Graphene based compounds are known to be good candidates as carbonaceous materials with high surface area,[17] high adsorption capacity,[18] and moderate acidic properties.[19] Thus, in this study, reduced graphene oxide (rGO) is selected as a component of a highly efficient, solid acid catalyst composite.

Titanium dioxide is a versatile material due to its high chemical stability, non-toxicity, low cost, and excellent photocatalytic properties.[20] Additionally, TiO_2 is known to show acidic properties especially when doped or coupled with other substances. Gardy J. *et al.* reported a transesterification catalytic process carried out with SO_4-Fe-Al-TiO_2 solid acid catalysts. Their report showed a significant increase in the acidity of TiO_2 upon coupling with other substances. Another study on acid catalysed dehydration of isobutanol carried out with TiO_2/SiO_2 was reported by Buniazet, Z. et al.[21] Furthermore, W^{6+} and Mo^{6+} can increase the Lewis acidity of TiO_2 with compared to other transition metal dopants such as Mn^{3+}/Mn^{4+}.[22,23]

Acetalization is the most popular method used for carbonyl protection which is important for multi-step organic synthesis in the presence of multiple functional groups. Furthermore, ketal and acetal compounds made as a result of acetalization have applications in the fields of organic synthesis, medicinal,[24] carbohydrate chemistry,[25] cosmetic fragrances,[26–29] and bio-based solvent synthesis.[30] However, the industrial applications of ketals are limited as the conventional method used is the acetalization by acids such as H_2SO_4, dry HCl, trifluoroacetic acid, and p-toluene sulfonic acid which are corrosive, have a tedious work up in separating the products, and produce harmful byproducts.[31,32] Thus, there was plenty of room for the exploration of environmentally benign acid catalysts for acetalization. As a result, a wide variety of studies were done on Lewis acids,[33–36] organic complexes,[37–40] metal complexes of precious metals (Pd, Pt, Rh etc.),[41–44] heteropoly acids,[45–48] zeolites,[26–28,49] and mesoporous cellular foams.[50] However, the use of many of these materials have drawbacks such as difficulty in product separation (homogeneous catalysts), high cost, high reaction temperature, long reaction time, limited substrate scope, low yield, and poor selectivity. Thus, novel solid acid catalysts which can give rise to green, environmentally benign acetalization processes are needed.

[a] *Department of Chemistry, Unit 3060, 55, North Eagleville road, Storrs, CT 06269, USA.*
[b] *Institute of Materials Science, University of Connecticut, 97 North Eagleville Road, Unit 3136, Storrs, CT 06269, USA.*
Electronic Supplementary Information (ESI) available: PDF file

In this study, a novel, high surface area, mesoporous composite material consisting of molybdenum doped TiO_2 nanoparticles on reduced graphene oxide (Mo-TiO_2/ rGO) is synthesized which showed excellent catalytic activity for acetalization of cyclohexanone. The catalyst reusability, absence of toxic waste, excellent GC yield, and easy product separation makes this a green, industrially scalable process.

Results

Material characterization

The structural properties of the synthesized materials were investigated using powder X-ray diffraction (Figure 1a). The PXRD pattern of reduced graphene oxide showed 2 peaks at 2θ = 24.1 and 43.0 degrees which correspond to (002) and (110) planes (PDF card No. 00-026-1079). The formation of reduced graphene oxide from graphene oxide is confirmed by the shift in the peak corresponding to the (002) planes from 26.5 to 12.4 degrees. The composite material which is Mo doped TiO_2/ reduced graphene oxide showed characteristic PXRD peaks corresponding to TiO_2 at 25.1, 37.9, 47.8, 53.9, 62.4, and 69.2 degrees. These peaks correspond to (101), (004), (200), (105), (211), (204), and (220) planes of anatase TiO_2 (PDF card No.00-021-1272). However, the peaks of the composite are broader compared to those of pure TiO_2. The composite of TiO_2/ rGO also showed peaks corresponding to anatase TiO_2 where the transition metal dopant is absent.

Further characterization of the structure of the composite was carried out using Raman spectroscopy where the bands corresponding to reduced graphene oxide were prominent (Figure 1b). The characteristic D and G bands were seen in the composite material at 1360 and 1609 cm^{-1}. The intensities of the overtone bands (2D and D+D') were reduced upon composite formation. The intensities of the Raman bands corresponding to TiO_2 were comparatively lower than those of rGO and were seen as a small hump around 100 - 500 cm^{-1}.

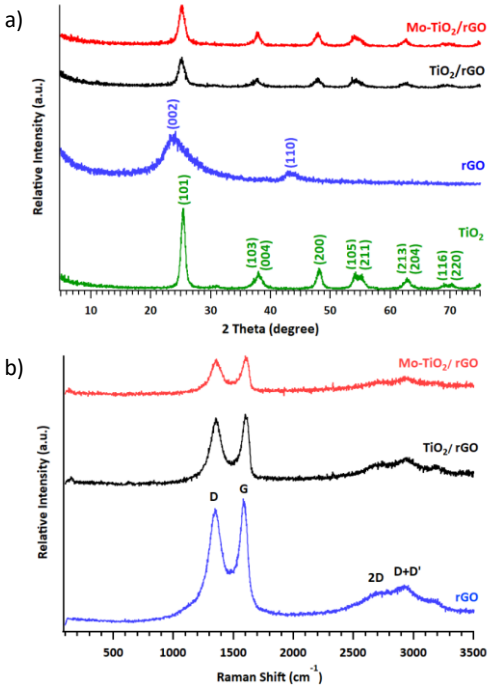

Figure 1. a) PXRD patterns b) Raman spectra of rGO, TiO_2/ rGO, and Mo-TiO_2/ rGO.

The surface areas and pore data of the synthesized materials were investigated using nitrogen adsorption isotherms. The BET isotherms of the composites TiO_2/ rGO and Mo-TiO_2/ rGO (Figure 2a) were type IV, H2 isotherms which are characteristic typical mesoporous materials. For the comparison the BET isotherms of rGO and pure TiO_2 are given in supplementary information Figure 1a and 2a. The highest BET surface area, which is 242 m^2/g was obtained for the composite Mo-TiO_2/ rGO. The BJH pore size distribution curves for all rGO, TiO_2 (supplementary information Figure 1b and 2b), TiO_2/ rGO, and Mo-TiO_2/ rGO (Figure 2b) showed monomodal pore size distribution curves where the average pore diameters were between 3 to 5 nm. The surface areas, average pore diameters, and pore volumes of the materials are listed in Table 1.

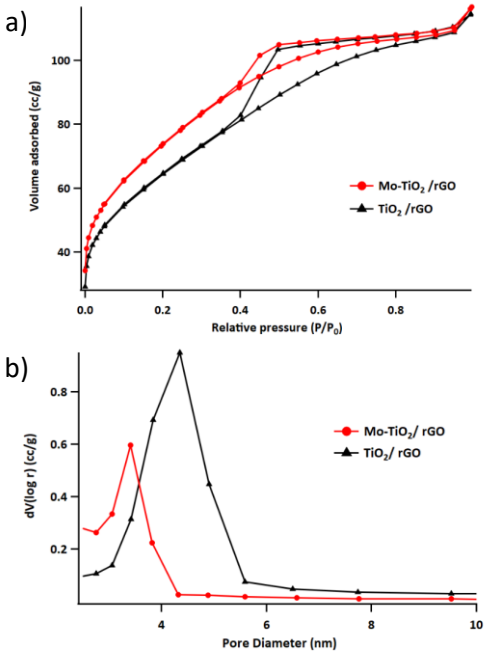

Figure 2. a) BET isotherms b) BJH pore size distribution curves of TiO_2/ rGO and Mo-TiO_2/ rGO.

Table 1. BET and BJH pore data of the synthesized materials.

Material	BET surface area (m^2/g)	BJH average pore diameter (nm)	BJH pore volume (cc/g)
TiO_2	36	3.8	0.05
rGO	104	3.8	0.65
TiO_2/ rGO	230	3.4	0.17
Mo-TiO_2/ rGO	263	3.4	0.16

The particle morphologies, sizes and distributions were investigated by SEM (Figure 3) where, randomly aggregated reduced graphene oxide sheets were observed. Upon addition of TiO_2 and Mo-doped TiO_2, the particles were embedded on the reduced graphene sheets. The EDX mapping (Figure 4) showed homogeneous distributions of Mo and TiO_2 throughout the composite material. Moreover, the atomic percentage calculated using EDX was 5% Mo with respective to Ti.

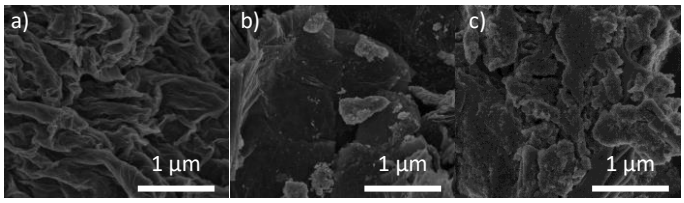

Figure 3. SEM images of a) rGO b) TiO_2/ rGO c) Mo-TiO_2/ rGO.

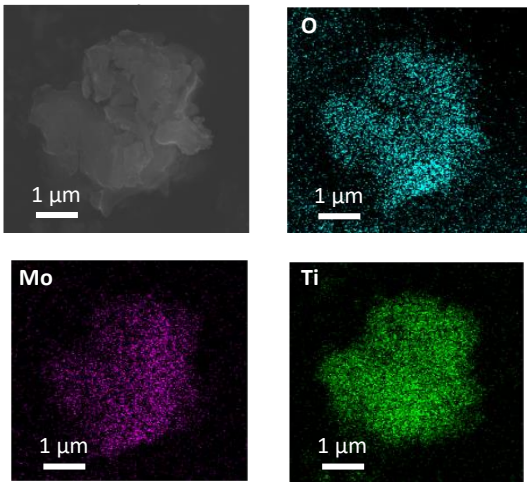

Figure 4. EDX mapping data of Mo-TiO_2/ rGO composite.

Further analyses of the particle sizes and distributions were carried out with HR-TEM where the thin sheets of reduced graphene oxide were clearly visible (Figure 5). TiO_2 and Mo doped TiO_2 particles are homogeneously distributed on the surface of reduced graphene oxide sheets. The SAED pattern of rGO (Figure 6a) showed the presence of (002) and (110) planes where the planes corresponding to TiO_2 were seen in the SAED patterns of TiO_2/ rGO and Mo-TiO_2/ rGO. The crystal planes (101) and (004) of TiO_2 were observed as lattice fringes in the HR-TEM image (Figure 7) of Mo-TiO_2/ rGO composite where the corresponding d spacing values were 0.35 nm and 0.23 nm. Similar to SEM EDS, TEM mapping (Figure 8) also confirmed that the Mo atomic percentage with respective to TiO_2 is 5%.

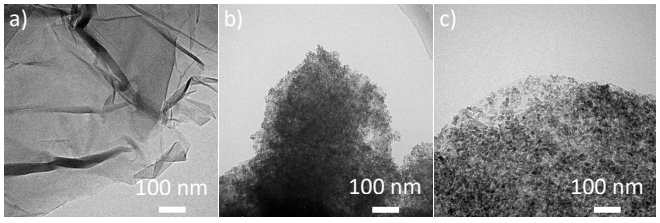

Figure 5. HR-TEM images of a) rGO b) TiO_2/ rGO c) Mo-TiO_2/ rGO.

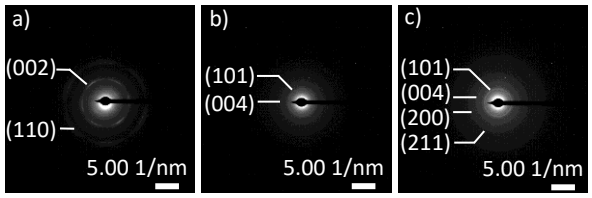

Figure 6. SAED patterns of a) rGO b) TiO_2/ rGO c) Mo-TiO_2/ rGO.

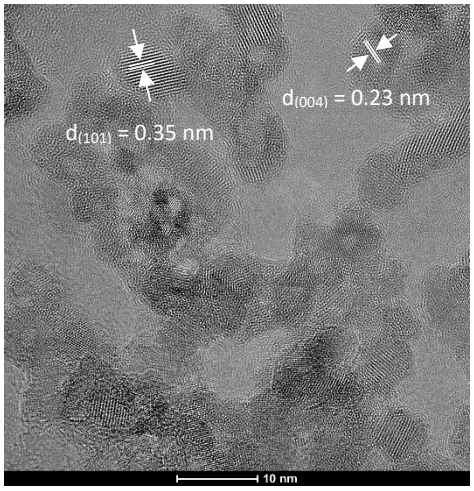

Figure 7. HR-TEM images with lattice fringes of Mo-TiO_2/ rGO.

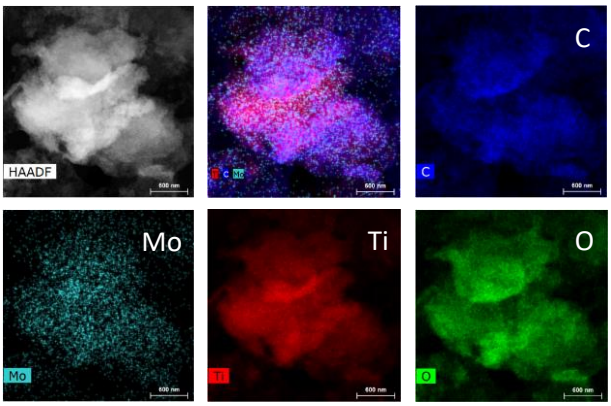

Figure 8. TEM mapping data of Mo-TiO_2/ rGO.

The thermogravimetric analysis (Figure 9) of Mo-TiO_2/ rGO composite showed a 78% mass loss which was similar to that of TiO_2/ rGO. This confirmed the mass loss is due to the removal of excess water and CO_2 generated from the TiO_2 counterpart. The mass loss of rGO was 3% and is due to the loss of adsorbed water and CO_2 species present in rGO.

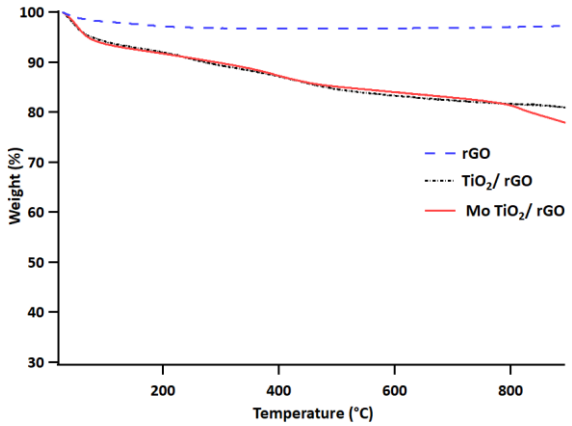

Figure 9. TGA data of rGO, TiO_2/ rGO, and Mo-TiO_2/ rGO.

The X-ray photoelectron spectrum of C 1s of the Mo-TiO_2/ rGO composite (Figure 10 a) exhibited peaks corresponding to C=C (284.6 eV), C–O (285. 3 eV), C=O (286.1 eV), and O–C=O (289.3 eV).[51–53] The peaks corresponding to O 1s (Figure 10 b) were at 530.5, 532.2, and 531.9 eV which confirmed the presence of lattice oxygen (O^{2-}) of TiO_2, surface hydroxyl groups, and chemisorbed water.[54,55] The peaks at 457.8, 459.2, and 464.9 eV (Figure 10 c) correspond to Ti^{3+} ($2p_{3/2}$), Ti^{4+} ($2p_{3/2}$), and Ti^{4+} ($2p_{1/2}$) respectively.[55–57] Only one peak is observed for Mo^{6+} ($3d_{5/2}$) at 232.9 eV (Figure 10 d).[57,58]

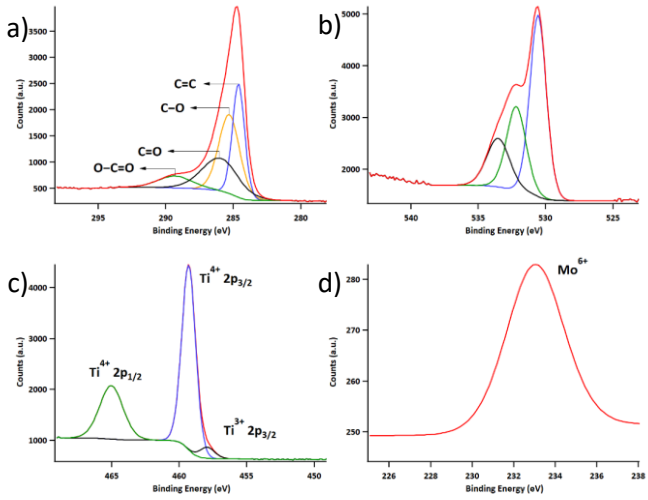

Figure 10. XP spectra of a) C 1 s b) O 1s c) Ti 2p d) Mo 3d in Mo-TiO_2/ rGO composite.

The acidic site density calculations (Table 2) showed that the Mo-TiO_2/ rGO composite has a higher density of weak acid sites with compared to pure rGO and TiO_2/ rGO composite. The strong acidic sites of all the materials were the same which shows that the strong acidic sites are present only in the rGO sheets. The differences in the acidic site densities are significant as compared to literature reported values.[1,59,60]

Table 2. Acidity of the composites calculated using neutralization titrations.

Material	Strong acidic groups (mmol/g)	Weak acidic groups (mmol/g)	Total (mmol/g)
rGO	1.00	11.00	12.00
TiO_2/ rGO	1.00	11.15	12.15
Mo-TiO_2/ rGO	1.00	11.52	12.52

Catalytic reaction

The catalytic reaction for the formation of 1,1-dimethoxy cyclohexane (Scheme 1) was studied using the synthesized Mo doped TiO_2/ rGO composite material. The coupling of methanol and cyclohexanone occurs within 30 minutes with excellent GC yield and selectivity. The reaction conditions such as catalyst loading, reaction temperature, reaction time, and the molar ratio between the reactants were optimized (Figure 11). The reaction proceeds with an excellent GC yield, selectivity, and turnover frequency at 0°C, 20°C, and 100°C. Thus, the optimized reaction conditions were found to be 10 mg of catalyst, 20°C, 1:10 cyclohexanone to methanol molar ratio, and 30 minutes. The catalyst is reusable up to 4 reaction cycles without losing significant activity (Figure 12 a). The catalyst leaching test was performed by removing the catalyst after 5 minutes and proceeding the reaction in the absence of the catalyst (Figure 12 b). As no catalyst leaching was observed, the heterogeneity was confirmed. The product formed was filtered an analyzed with GC-MS (Supplementary information Figure 3). The substrate scope was analyzed using different ketone and alcohol compounds (Table 2). The reaction was carried out using pure rGO and TiO_2/ rGO composite where the GC yields were 74% and 78%. Furthermore, the reaction was carried out without catalyst, with commercial MoO_3, and TiO_2 as additional control experiments where the obtained GC yields were 0%. For comparison, commercial zeolites were used as the catalyst for the acetalization reaction and the products were analyzed using GCMS (Supplementary information Figure 4) where lower yields (8%, 0%) were observed (Supplementary information Table 1).

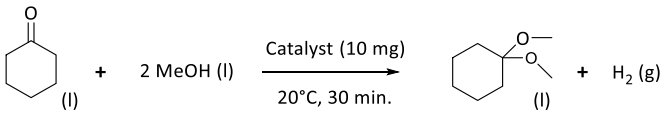

Scheme 1. Synthesis of 1,1-dimethoxy cyclohexane.

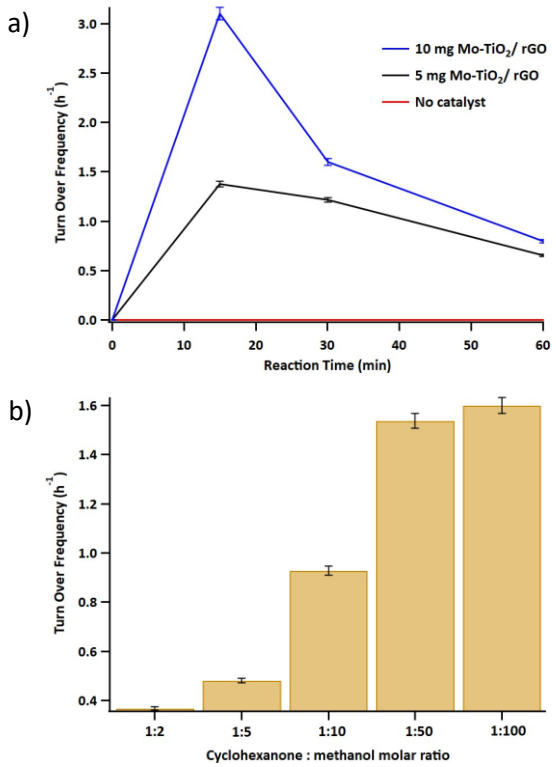

Figure 11. Optimization of a) catalyst loading and reaction time b) molar ratio between reactants.

[Reaction conditions a) 0.1 mmol cyclohexanone, 0.5 mL methanol, 20°C b) 10 mg catalyst, 20°C, 30 minutes].

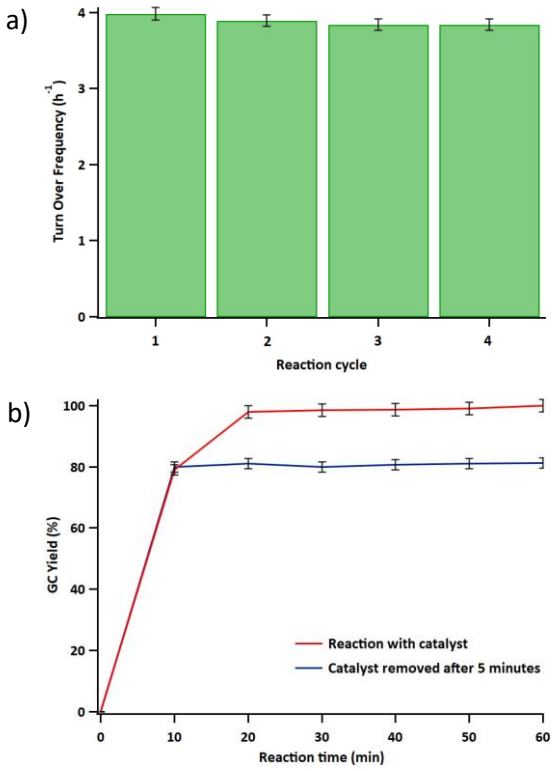

Figure 12 a) Catalyst reusability test b) catalyst leach test.

Reaction conditions a) 0.1 mmol cyclohexanone, 0.5 mL methanol, 20°C, 10 mg catalyst, 10 minutes b) 0.1 mmol cyclohexanone, 0.5 mL methanol, 10 mg catalyst, 20°C, 30 minutes].

Table 3. Substrate scope for the acetalization reaction.

Reactant 1	Reactant 2	Product	TOF[(a)] (h^{-1})
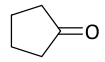		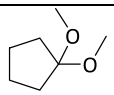	1.6
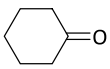		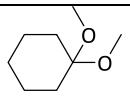	1.6
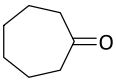		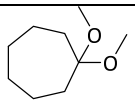	0.3
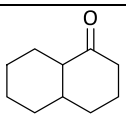		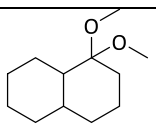	1.2
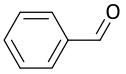		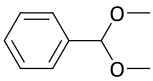	1.6
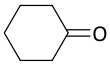		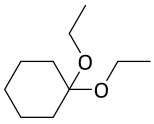	0.9
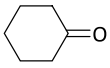		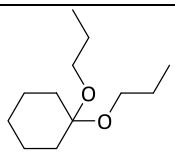	1.0
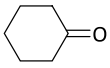	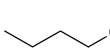	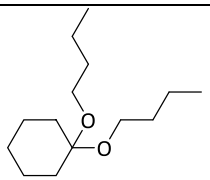	1.2
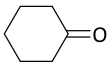		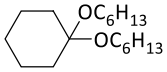	1.6
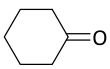	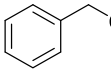	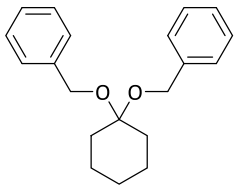	0.9
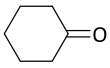	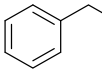	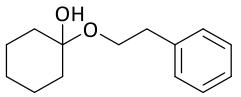	1.2

[(a)]TOF = turnover frequency = mols of cyclohexanone converted to dimethoxy cyclohexane per mol of acidic sites in the catalyst per hour.

[Reaction conditions a) 0.1 mmol ketone/ aldehyde, 0.5 mL alcohol, 20°C, 10 mg catalyst, 30 minutes].

Discussion

The well-developed sheet structure of graphite is shown by the sharp peak of its PXRD pattern and upon oxidation, the exfoliated graphene oxide sheets are restacked and peak broadening is observed (Supplementary information Figure 5). The increase in d spacing of graphene oxide is due to the formation of epoxy, hydroxyl, carbonyl, and carboxyl groups upon oxidation.[61,62] Upon reduction, the oxygen containing functional groups are removed and the reduced graphene sheets are arranged randomly. As a result, the PXRD peak is broad as compared to graphite. The reason for the poor arrangement of the rGO sheets may be due to the presence of single or few layers.[61] In rGO the peak with less intensity which is seen at 43.0 degrees is due to the turbostratic band of disordered carbon materials.[63] The peak broadening of the PXRD pattern of Mo-TiO_2/ rGO is due to the presence of carbonaceous species in the form of reduced graphene oxide. The PXRD peaks of rGO in the composite might be masked from the peaks of the crystalline TiO_2 counterpart. The absence of PXRD peaks corresponding to molybdenum could be due to the insertion of Mo^{6+} ions into the TiO_2 lattice replacing some of the Ti^{4+} ions. Another possibility is that molybdenum can be present in a non-crystalline or poorly crystalline phase.

The Raman spectrum of graphite (Supplementary information Figure 6) showed a large intense peak at 1585 cm^{-1} which corresponds to the characteristic G band. This is due to in plane sp^2 carbon vibrations and a doubly-degenerate phonon modes with E_{2g} symmetry at the Brillouin zone centre.[64] The D band corresponds to sp^3 carbons, structural defect sites, or edge planes. The intensity of the D band is lower in graphite and upon oxidation the intensity increases due to the presence of a higher number of defects. The peak present at 2705 cm^{-1} is known as the 2D band and arises due to the presence of second-order zone-boundary phonons. [62,65] The position and the shape of the 2D band can be used to determine the number of layers (single layer or multi-layer). Furthermore, the 2D peak could be sensitive to doping as well.[64] In this study, the 2D bands of graphene oxide, reduced graphene oxide, and composite materials showed similar shapes and intensities. As all the 2D bands were broad, the formation of multi layered structures is confirmed. The characteristic Raman bands corresponding to pure TiO_2 (Supplementary information Figure 7) were observed at 145, 198, 399, 516, and 640 cm^{-1}. In the composite materials the peak intensities of the Raman bands corresponding to TiO_2 were lower compared to the bands corresponding to rGO.

Upon formation of rGO, the porous nature and surface area increase due to the stirring and hydrothermal treatment. The initial surface area of graphite (6 m^2/g) increases up to 104 m^2/g. When the TiO_2/ rGO composite is formed, the surface area is increased due to the presence of TiO_2 nano particles with high surface area. However, when Mo dopant is added the aggregation of TiO_2 particles is reduced and as a result, the surface area has further increased up to 263 m^2/g. This result was observed in SEM and TEM images as well. When only TiO_2 particles are present on rGO sheets, particle aggregation was seen where Mo-doped TiO_2 particles were homogeneously distributed.

The XP spectra of C 1s and O 1s of the Mo-TiO_2/ rGO composite showed the presence of characteristic C-C, C=O, lattice O, and surface hydroxyl groups which are in accordance with literature reported data. However, the bands of Ti 2p showed the presence of Ti^{3+} $2p_{3/2}$ (457.8 eV) and a shift in the Ti^{4+} $2p_{3/2}$ (459.2 eV) peak to a higher value. The reported binding energy of Ti^{4+} $2p_{3/2}$ is 458.5 eV.[57,66] There could be several reasons for the afore mentioned shift in the Ti^{4+} peak and for the presence of multivalent Ti. The presence of a high valent dopant (Mo^{6+}) in the TiO_2 lattice would produce multiple oxidation states of Ti, excess oxygen, or Ti^{4+} vacancies to maintain the total charge balance.[57]

The proposed reaction mechanism for the acetalization (Scheme 2) shows that the acidity of the catalyst is the key factor for the catalytic acetalization reaction. The afore mentioned proposal is confirmed by the GC yields of the acetalization when rGO, TiO_2/ rGO, and Mo-TiO_2/ rGO materials were used as catalysts. The material with the highest number of acidic sites showed the highest activity towards the reaction. In the rGO counterpart, the COOH groups act as strong acidic groups and carbonyl, epoxy, hydroxyl groups are weak acidic sites.[1] In the Mo doped TiO_2 counterpart, the surface hydroxyl groups act as weak acidic groups which further facilitate the catalytic reaction. The reaction mechanism was supported by the reactions done with the ion exchanged Mo-TiO_2/ rGO catalyst where only 85% of GC yield was obtained when the strong acidic sites were exchanged with NaCl and 0% GC yield was obtained when all the strong and weak acidic sites were exchanged. Thus, weak acidic sites are responsible for the acetalization reaction.

According to a reviewer, one could calculate the size of the acidic sites using the surface area of the materials. However, the above phenomenon could not be the case for the materials synthesized in this study as the total surface areas were measured. The total surface area consists of both acidic and non-acidic sites. Thus, the total areas are not the active surface areas. Furthermore, the size of the acidic sites varies as they can be different types of Brønsted acidic sites (form reduced graphene oxide surface and metal oxide surfaces) and Lewis acidic sites (from Ti and Mo). Thus, the calculation of the size of the acidic sites using surface area would not be accurate in this study. However, to estimate the sizes of the acid sites present, different types of bases were used. The kinetic diameters of the bases used are as follows; ammonia 0.26 nm, pyridine 0.54 nm, and 2,6-dimethylpyridine 0.67 nm.[67,68] After neutralizing the acid sites with the bases given above, the catalytic reaction was performed. The yields for the catalytic reactions after neutralizing acid sites with ammonia, pyridine, and 2,6-dimethylpyridine are 0%, 47%, and 19% respectively. All the acid sites are neutralized with ammonia due to the smaller size. Thus, the size of the acid sites should be similar or larger than ammonia. Pyridine has deactivated only a portion of acid sites where 2,6-dimethylpyridine has neutralized the surface acidic sites which are accessible due to the large kinetic diameter.

A reviewer has suggested that the size of the acid sites may be important in these reactions. We are not aware of methods that have been developed to do this. One can envision taking different sizes and shapes of base titrants and quantitatively comparing differences between these species. That may lead to information about the exact size of acid sites. However, such studies will need to be developed and are beyond the scope of this paper.

The post catalyst analyses were performed to investigate the reusability and to monitor the changes of the catalysts after 4 catalytic reaction cycles. The PXRD (Supplementary information Figure 8), SEM (Supplementary information Figure 9), TEM (Supplementary information Figure 10), and XPS (Supplementary information Figure 11) analyses showed that there are no significant differences in Mo-TiO_2/ rGO before and after the reaction. However, after 4 reaction cycles the nitrogen sorption isotherms (Supplementary information Figure 12) exhibited a decrease in surface area from 263 to 240 m^2/g. This could be the reason for the slight reduction in activity after 4 reaction cycles.

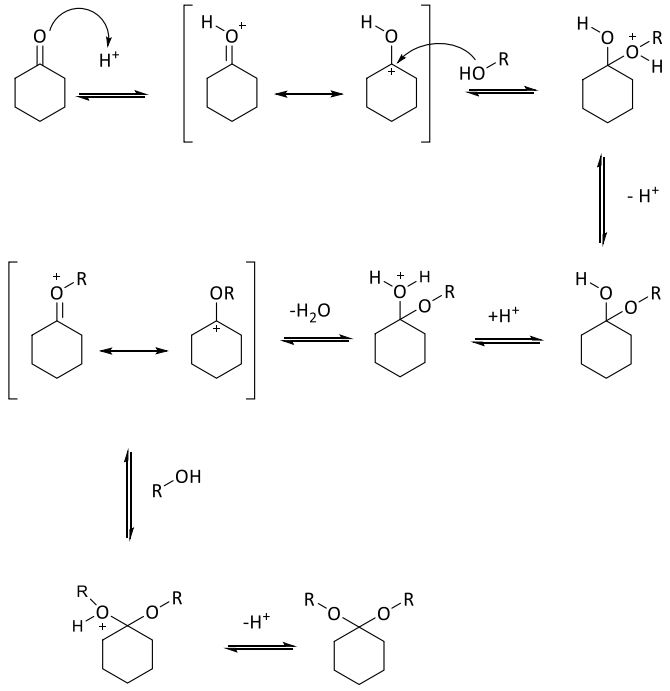

Scheme 2. Proposed reaction mechanism for the acetalization

Experimental

Materials

All the chemicals were used as received. For the synthesis of graphene oxide, potassium permanganate (99.0%), sulfuric acid (95.0-98.0%), and hydrogen peroxide (30 wt.% in H_2O) were purchased from Sigma-Aldrich. Graphite powder and sodium nitrate were purchased from Asbury Graphite Mills Inc. and Janssen Chimica respectively. As the precursors for the composite, titanium (IV) isopropoxide (97%) was purchased from Alfa Aeser while hydrochloric acid (37%) and ethanol (99.5%) were purchased from Sigma-Aldrich. Anhydrous acid molybdic was purchased from (99.8%) Bakers Analyzed. For the acid site determination, sodium chloride and sodium hydroxide were purchased from J.T. Baker and Sigma Aldrich.

Methods

Synthesis of graphene oxide (GO)

For the synthesis of graphene oxide Hummer's method[69] was used where, graphite (1 g), sodium nitrate (1 g), and concentrated sulfuric acid (50 mL) were stirred in an ice bath for 30 minutes. Upon addition of potassium permanganate (8 g) to the mixture, the solution turned in to green. The green sol was further stirred for 30 minutes in the ice bath and was transferred in to a 40°C water bath followed by stirring for another 90 minutes to ensure the complete oxidation of graphite. Then, distilled water (100 mL) was added slowly to the resultant green sol and stirred for 30 minutes. The reaction was quenched by adding hydrogen peroxide (12 mL) which turned the mixture in to a golden-brown sol. After adding more distilled water (100 mL), the brown precipitate formed was separated from the yellow colored supernatant and the brown precipitate was washed with distilled water until it is neutral. The resultant golden yellow colored solution was used for the synthesis of the composite. To obtain graphene oxide powder the solution was dried at 80°C.

Synthesis of Mo doped TiO_2 reduced graphene oxide composite

First, titanium (IV) isopropoxide (3 mL) was added dropwise to a mixture of ethanol (2.5 mL) and hydrochloric acid (3.5 mL). To the resultant solution, graphene oxide (10 wt.% of Ti) solution was added followed by the addition of anhydrous acid molybdic (5 mol% of Ti). The solution mixture was stirred for 1 hour and placed in a Teflon lined autoclave followed by the hydrothermal treatment at 150°C for 12 hours. The black colored powder obtained was separated and vacuum dried overnight. To synthesize TiO_2/ rGO composite, the procedure given above was followed without the molybdenum dopant.

Catalytic reaction

The catalytic acetalization was monitored by the formation of 1,1-dimethoxy cyclohexane from the reaction between cyclohexanone and methanol. For the optimized reaction conditions, cyclohexanone (0.1 mmol) and methanol (0.5 mL) were stirred at room temperature for 30 minutes in the presence of Mo-TiO_2/ rGO catalyst (10 mg). The product formed was filtered and identified by GC-MS.

Acidity measurement

The neutralization titration method was used to calculate the surface strong acid and weak acid densities.[1,59,60] For the calculation of strong acid sites 0.10 g of Mo-TiO_2/ rGO was added to 100 mL of 1M NaCl (excess) and was stirred overnight. The supernatant was separated, and an aliquot was titrated with 0.1 M NaOH in the presence of phenolphthalein indicator. To calculate the combination of strong acid and weak acid sites, 100 mg of Mo-TiO_2/ rGO was mixed with 0.05 M NaOH and stirred overnight. An aliquot of the supernatant was back titrated with 0.1 M HCl in the presence of phenolphthalein indicator. As control experiments the acidic site densities of rGO and TiO_2/ rGO composite were calculated. The ion-exchanged Mo-TiO_2/ rGO catalyst was used in a generic reaction to investigate the effect of ion-exchange on the GC yield.

The size estimation of the acid sites was done using bases with different sizes. First, Mo-TiO_2/rGO powder (50 mg) was stirred for 8 hours with ammonia (0.5 mmol), pyridine (0.5 mmol), and 2,6-

dimethylpyridine (0.5 mmol) in separate containers. Then, the powder was separated and dried at 60°C. Catalytic reactions were performed using the resultant solid materials. Mo-TiO_2/rGO (10 mg), cyclohexanone (0.1 mmol), and methanol (0.5 mL) were stirred at room temperature for 30 minutes and the products were analyzed using GCMS.

Characterization

Structural characterization was performed using PXRD patterns obtained from a Rigaku Ultima IV diffractometer with Cu Kα radiation (λ = 1.5406 Å). The samples were scanned from 2θ = 2 to 75 degrees (rate of 2 degrees per minute) with a 44 kV beam voltage and 44 mA current. A Renishaw System 2000 microscope which is equipped with an Ar^+ ion laser excitation source (λ = 514 nm) was used for the Raman analysis. A Quantachrome Autosorb iQ_2 automated gas sorption analyser was used to obtain the nitrogen sorption isotherms which were used to calculate the surface areas and pore data. The samples were degassed (150°C – 4 hours) prior to the analysis and the Brunauer–Emmett–Teller (BET) isotherms were used to calculate the surface areas. The Barrett, Joyner, and Halenda (BJH) method which uses the desorption branch of the isotherms was used to determine pore diameters and pore volumes of the synthesized materials. The particle morphology and the distribution of TiO_2 on reduced graphene oxide sheets were analyzed using an FEI Nova NanoSEM 450 equipped with a high current Schottky gun which is operated at 2.0 kV. To analyze the distribution of TiO_2 and Mo on the surface and to calculate the atomic percentage of Mo with respect to Ti, energy dispersive X-ray (EDS) analysis was performed using an Oxford Aztec Energy Microanalysis system with an X-max 80 silicon drift detector. High-resolution transmission electron microscopic (HR-TEM) images were obtained to observe the reduced graphene oxide sheets and to further analyse the particle distribution, particle size, and atomic percentages using a Talos F200X microscope operating at 200 kV and equipped with an energy dispersive spectrometer (EDS). The thermogravimetric analyses were performed on a NETZSCH TG 209F1 Libra equipped with a NETZSCH QMS 403C mass spectrometer. The temperature range was from 27- 900°C with a ramp of 10°C min^{-1} under nitrogen atmosphere (flow rate 60 mL min^{-1}). A Quantum 2000 Scanning ESCA Microprobe (Physical Electronics Corporation -Division of ULVAC-PHI) with a monochromatic Al Kα X-ray (1486.6 eV) source with a beam diameter of 10 µm was used for the XPS analyses. The binding energy spectra were corrected based on assigning a C 1s peak to adventitious carbon ($E_{BINDING}$ = 284.8 eV) as a primary correction. The products obtained from the catalytic reaction were analyzed using an Agilent gas-phase chromatography-electron impact-quadrupole mass spectrometer (GC-MSD) 5975.

Conclusions

A novel, mesoporous composite material with high surface area (263 m^2/g) is fabricated via an *in-situ* hydrothermal synthesis method. The composite contains 5% Mo doped TiO_2 nanoparticles on reduced graphene oxide sheets. The catalytic acetalization reaction was monitored using the synthesis of 1,1, -dimethoxy cyclohexane as the generic reaction. The weak acidic sites of the composite material play a major role in the acetalization process. The catalyst heterogeneity, reusability, ambient reaction conditions, lower reaction time, reusability of excess reactants (alcohol), high GC yield, and selectivity make this a "green", industrially feasible process.

Conflicts of interest

There are no conflicts to declare.

Acknowledgements

This work was funded by the U.S. Department of Energy, Office of Basic Energy Sciences, Division of Chemical, Biological, and Geological Sciences, under Grant DE-FGO2- 86ER13622.A000. The TEM analyses were performed using the facilities in the UConn-Thermo Fisher Scientific Center for Advanced Microscopy and Materials Analysis (CAMMA). SLS acknowledges excellent discussions with Professor Abraham Clearfield over many years, especially concerning X-ray methods.

References

1 H. P. Gong, W. M. Hua, Y. H. Yue and Z. Gao, *Appl. Surf. Sci.*, 2017, **397**, 44–48.
2 A. N. Historic and C. Landmark, *Am. Chem. Soc.*, 2.
3 R. B. Borade and A. Clearfield, *J. Chem. Soc. Faraday Trans.*, 1995, **91**, 539–547.
4 R. B. Borade and A. Clearfield, *Stud. Surf. Sci. Catal.*, 1994, **84**, 661–668.
5 J. F. Haw, in *Physical Chemistry Chemical Physics*, 2002, vol. 4, pp. 5431–5441.
6 J. Bernholc, J. A. Horsley, L. L. Murrell, L. G. Sherman and S. Soled, *J. Phys. Chem.*, 1987, **91**, 1526–1530.
7 K. R. Venkatesh, J. Hu, C. Dogan, J. W. Tierney and I. Wender, *Energy & Fuels*, 1995, **9**, 888–893.
8 C. Tagusagawa, A. Takagaki, A. Iguchi, K. Takanabe, J. N. Kondo, K. Ebitani, S. Hayashi, T. Tatsumi and K. Domen, *Angew. Chemie - Int. Ed.*, 2010, **49**, 1128–1132.
9 B. Grzybowska-Świerkosz, *Mater. Chem. Phys.*, 1987, **17**, 121–144.
10 M. N. Timofeeva, *Appl. Catal. A Gen.*, 2003, 256, 19–35.
11 M. A. Hanif, S. Nisar and U. Rashid, *Catal. Rev.*, 2017, **59**, 165–188.
12 R. B. Borade and A. Clearfield, *Appl. Catal. A, Gen.*, 1992, **80**, 59–77.
13 J. Zhang, Y. Yan, Q. Chu and J. Feng, *Fuel Process. Technol.*, 2015, **135**, 2–5.
14 Z. Zhu, Z. Xie, Y. Chen, R. Wang and Y. Yao, *React. Kinet. Catal. Lett.*, 2000, **70**, 379–388.
15 Z. Wang, J. M. Heising and A. Clearfield, *J. Am. Chem. Soc.*, 2003, **125**, 10375–10383.
16 T. Okuhara, *Chem. Rev.*, 2002, **102**, 3641–3666.
17 M. J. Allen, V. C. Tung and R. B. Kaner, *Chem. Rev.*, 2010, **110**, 132–145.

18 G. Liao, S. Chen, X. Quan, H. Yu and H. Zhao, *J. Mater. Chem.*, 2012, **22**, 2721–2726.
19 D. R. Dreyer, H.-P. Jia and C. W. Bielawski, *Angew. Chemie Int. Ed.*, 2010, **49**, 6686–6686.
20 J. G. Huang, X. T. Guo, B. Wang, L. Y. Li, M. X. Zhao, L. L. Dong, X. J. Liu and Y. T. Huang, *J. Spectrosc.*, 2015, **2015**, 1–8.
21 Z. Buniazet, J. Couble, D. Bianchi, M. Rivallan, A. Cabiac, S. Maury and S. Loridant, *J. Catal.*, 2017, **348**, 125–134.
22 S. Liu, E. Guo and L. Yin, *J. Mater. Chem.*, 2012, **22**, 5031–5041.
23 R. Nasi, T. Gadhi, S. Esposito, S. Hernández, M. Armandi and B. Bonelli, *Mo doped TiO2 nanoparticles for photocatalytic dye degradation*, 2017.
24 Y. M. Choi-Sledeski and C. G. Wermuth, in *The Practice of Medicinal Chemistry: Fourth Edition*, Academic Press, 2015, pp. 657–696.
25 P. Grice, S. V. Ley, J. Pietruszka, H. M. I. Osborn, H. W. M. Priepke and S. L. Warriner, *Chem. - A Eur. J.*, 2006, **3**, 431–440.
26 M. J. Climent, A. Corma and A. Velty, *Appl. Catal. A Gen.*, 2004, **263**, 155–161.
27 M. J. Climent, A. Velty and A. Corma, *Green Chem.*, 2002, **4**, 565–569.
28 M. J. Climent, A. Corma, A. Velty and M. Susarte, *J. Catal.*, 2000, **196**, 345–351.
29 E. Pérez-Mayoral, R. M. Martín-Aranda, A. J. López-Peinado, P. Ballesteros, A. Zukal and J. Čejka, *Top. Catal.*, 2009, **52**, 148–152.
30 L. Moity, A. Benazzouz, V. Molinier, V. Nardello-Rataj, M. K. Elmkaddem, P. De Caro, S. Thiébaud-Roux, V. Gerbaud, P. Marion and J. M. Aubry, *Green Chem.*, 2015, **17**, 1779–1792.
31 S. J. Yang, X. X. Du, L. He and J. T. Sun, *J. Zhejiang Univ. Sci.*, 2005, **6 B**, 373–377.
32 J. L. Dong, L. S. H. Yu and J. W. Xie, *ACS Omega*, 2018, **3**, 4974–4985.
33 Y. Zong, L. Yang, S. Tang, L. Li, W. Wang, B. Yuan and G. Yang, *Catalysts*, , DOI:10.3390/catal8020048.
34 M. Bakos, Á. Gyömöre, A. Domján and T. Soós, *Angew. Chemie Int. Ed.*, 2017, **56**, 5217–5221.
35 D. J. M. Lyons, R. D. Crocker, D. Enders and T. V. Nguyen, *Green Chem.*, 2017, **19**, 3993–3996.
36 N. Hamada, K. Kazahaya, H. Shimizu and T. Sato, *Synlett*, 2004, 1074–1076.
37 B. Karimi, H. Hazarkhani and J. Maleki, *Synthesis (Stuttg).*, 2005, 279–285.
38 M. Kotke and P. R. Schreiner, *Tetrahedron*, 2006, **62**, 434–439.
39 B. Karimi, H. Seradj and G. R. Ebrahimian, *Synlett*, 1999, 1456–1458.
40 D. Li, F. Shi, J. Peng, S. Guo and Y. Deng, *Chem. Technol. Biotechnol*, 1981, **50**, 3582–3585.
41 M. Cataldo, E. Nieddu, R. Gavagnin, F. Pinna and G. Strukul, *J. Mol. Catal. A Chem.*, 1999, **142**, 305–316.
42 J. Zhou, Z. Dong, H. Yang, Z. Shi, X. Zhou and R. Li, *Appl. Surf. Sci.*, 2013, **279**, 360–366.
43 J. J. Wilson and S. J. Lippard, *Chem. Rev.*, 2014, **114**, 4470–95.
44 S. R. Khan and B. M. Bhanage, *Tetrahedron Lett.*, 2013, **54**, 5998–6001.
45 I. V Kozhevnikov, *Chem. Rev.*, 1998, **98**, 171–198.
46 L. Chen, B. Nohair, D. Zhao and S. Kaliaguine, *ChemCatChem*, 2018, **10**, 1918–1925.
47 G. Jinzhang, L. Shengying, Y. Wu, Z. Guohu, B. Lili and S. Li, *Rare Met.*, 2007, **26**, 1–7.
48 B. R. Jermy and A. Pandurangan, *Appl. Catal. A Gen.*, 2005, **295**, 185–192.
49 I. Rodriguez, M. J. Climent, S. Iborra, V. Fornés and A. Corma, *J. Catal.*, 2000, **192**, 441–447.
50 K. Stawicka, A. E. Díaz-Álvarez, V. Calvino-Casilda, M. Trejda, M. A. Bañares and M. Ziolek, *J. Phys. Chem. C*, 2016, **120**, 16699–16711.
51 C. Song, S.-J. Park and S. Kim, *J. Electrochem. Soc.*, 2016, **163**, F668–F676.
52 M. Khan, A. H. Al-Marri, M. Khan, M. R. Shaik, N. Mohri, S. F. Adil, M. Kuniyil, H. Z. Alkhathlan, A. Al-Warthan, W. Tremel, M. N. Tahir and M. R. H. Siddiqui, *Nanoscale Res. Lett.*, 2015, **10**, 1–9.
53 F. Tuz Johra, J. Lee and W.-G. Jung, *J. Ind. Eng. Chem.*, 2014, **20**, 2883–2887.
54 O. Avilés-García, J. Espino-Valencia, R. Romero, J. L. Rico-Cerda, M. Arroyo-Albiter and R. Natividad, *Fuel*, 2017, **198**, 31–41.
55 Y. Yang, L. Luo, M. Xiao, H. Li, X. Pan and F. Jiang, *Mater. Sci. Semicond. Process.*, 2015, **40**, 183–193.
56 S. Wang, L. N. Bai, H. M. Sun, Q. Jiang and J. S. Lian, *Powder Technol.*, 2013, **244**, 9–15.
57 K. Bhattacharyya, J. Majeed, K. K. Dey, P. Ayyub, A. K. Tyagi and S. R. Bharadwaj, *J. Phys. Chem. C*, 2014, **118**, 15946–15962.
58 A. Q. Khan, S. Yuan, S. Niu, L. Zheng, W. Li and H. Zeng, *Opt. Express*, 2017, **25**, A539.
59 S. Suganuma, K. Nakajima, M. Kitano, D. Yamaguchi, H. Kato, S. Hayashi and M. Hara, *J. Am. Chem. Soc.*, 2008, **130**, 12787–12793.
60 K. R. Benak, L. Dominguez, J. Economy and C. L. Mangun, *Carbon N. Y.*, 2002, **40**, 2323–2332.
61 N. M. S. Hidayah, W. W. Liu, C. W. Lai, N. Z. Noriman, C. S. Khe, U. Hashim and H. C. Lee, in *AIP Conference Proceedings*, 2017, vol. 1892, p. 150002.
62 M. Wojtoniszak, X. Chen, R. J. Kalenczuk, A. Wajda, J. Łapczuk, M. Kurzewski, M. Drozdzik, P. K. Chu and E. Borowiak-Palen, *Colloids Surfaces B Biointerfaces*, 2012, **89**, 79–85.
63 F. W. Low, C. W. Lai and S. B. Abd Hamid, *Ceram. Int.*, 2015, **41**, 5798–5806.
64 D. Naumenko, V. Snitka, B. Snopok, S. Arpiainen and H. Lipsanen, *Nanotechnology*, 2012, **23**, 465703.
65 A. C. Ferrari, *Solid State Commun.*, 2007, **143**, 47–57.
66 B. Bharti, S. Kumar, H. N. Lee and R. Kumar, *Sci. Rep.*, 2016, **6**, 32355.
67 M. Kanezashi, A. Yamamoto, T. Yoshioka and T. Tsuru, *AIChE J.*, 2010, **56**, 1204–1212.

68 K. Góra-Marek, K. Tarach and M. Choi, *J. Phys. Chem. C*, 2014, **118**, 12266–12274.
69 W. S. Hummers and R. E. Offeman, *J. Am. Chem. Soc.*, 1958, **80**, 1339.

Table of Contents

A novel, mesoporous molybdenum doped titanium dioxide-reduced graphene oxide composite is synthesized as a highly efficient heterogeneous solid acid catalyst.